DALTON

Synthesis and characterization of the centred icosahedral cluster series $[Au_9M^{IB}{}_4Cl_4(PMePh_2)_8][C_2B_9H_{12}]$, where M^{IB} = Au, Ag or Cu

Royston C. B. Copley [a] **and D. Michael P. Mingos** *[,b]

[a] *Inorganic Chemistry Laboratory, University of Oxford, South Parks Road, Oxford OX1 3QR, UK*
[b] *Department of Chemistry, Imperial College of Science, Technology and Medicine, South Kensington, London SW7 2AY, UK*

The compounds $[Au_9M^{IB}{}_4Cl_4(PMePh_2)_8][C_2B_9H_{12}]$ (M^{IB} = Au, Ag or Cu) have been prepared from solutions of $[Au_{11}(PMePh_2)_{10}][C_2B_9H_{12}]_3$ by the addition or formation *in situ* of $[M^{IB}Cl(PMePh_2)]$. The reaction is believed to take place *via* the intermediate cations $[Au_{11}M^{IB}{}_2Cl_2(PMePh_2)_{10}]^{3+}$ and $[Au_{10}M^{IB}{}_3Cl_3(PMePh_2)_9]^{2+}$. The final products have been characterized by FAB mass spectrometry, electronic spectroscopy and ^{31}P-$\{^1H\}$, ^{11}B-$\{^1H\}$ and ^1H NMR spectroscopy. Single-crystal X-ray diffraction studies on $[Au_9Ag_4Cl_4(PMePh_2)_8]$-$[C_2B_9H_{12}]\cdot H_2O\cdot 0.5CH_2Cl_2$ and $[Au_9Cu_4Cl_4(PMePh_2)_8][C_2B_9H_{12}]\cdot CH_2Cl_2$ have been carried out. The cations of these compounds contain centred icosahedral metal frameworks and in both cases the cages have approximate C_{2v} symmetry: the silver and copper atoms, associated with the halide ligands, occupy identical positions. A gold atom sits at the interstitial site. The cations cannot be superimposed due to differences in the ligand packing. Comparable Au–Au bond lengths in the two structures are very similar and, given the large differences that are seen between the Au–Ag and the Au–Cu bond lengths, the Ag–Cl and Cu–Cl moieties can be visualized as moving relative to one another along radial vectors.

A recurring structural theme in gold cluster chemistry is the centred icosahedron and geometries based on it: many of the homonuclear cluster compounds containing less than thirteen metals have cage architectures based on fragments of this.[1] The first structural characterization of a complete centred icosahedron was reported in 1981.[2] The compound $[Au_{13}Cl_2(PMe_2Ph)_{10}][PF_6]_3$ represented the realization of a theoretical prediction[3] and was prepared by the reduction of [AuCl(PMe_2Ph)] with $[Ti(\eta\text{-}C_6H_5Me)_2]$. The reaction proceeded *via* a brown intermediate that was never unequivocally characterized. Many other Au_{13} compounds were prepared at this time and on the basis of NMR studies were believed to contain the same metal framework.[4,5] In addition to phosphines, the ligands in the Au_{13} clusters generally included either two, three or four halides or pseudo-halides. The phosphine $PMePh_2$ was used in preference to PMe_2Ph because the resulting compounds were found to be more stable. The products containing this phosphine were characterized on the basis of microanalyses and NMR spectroscopy and are summarized in Scheme 1. The cation $[Au_{13}Cl_4(PMePh_2)_8]^+$ represents the homonuclear member of the cluster series discussed in this paper. The only other Au_{13} cluster cation to be structurally characterized is $[Au_{13}(dppp)_6]^{n+}$ [dppp = $Ph_2P(CH_2)_3PPh_2$] which also contains the centred icosahedral skeleton.[6]

Cluster compounds containing heteronuclear M^{IB}–M^{IB} bonds are not common and by far the largest category of these are the bimetallic gold–silver supraclusters championed by Teo.[7,8] They have generally been prepared by reducing monomers containing the two metals in EtOH using $NaBH_4$. The icosahedral geometry is found to be a primary building block and all the clusters can be visualized as being made from linking centred Au_7Ag_6 icosahedra by means of vertex sharing. A number of interesting points arise from the study of the bimetallic gold–silver supraclusters: (*i*) gold atoms always occupy the vertex-sharing positions and are at the centres of the basic icosahedra; (*ii*) gold atoms on the periphery of the cluster are always bonded to phosphine groups; and (*iii*) silver atoms are always bonded to halide ligands, either terminal, bridging or both. Teo and Zhang[10] explained these preferences in terms of the Pauling electronegativities of gold (2.54) and silver (1.93).

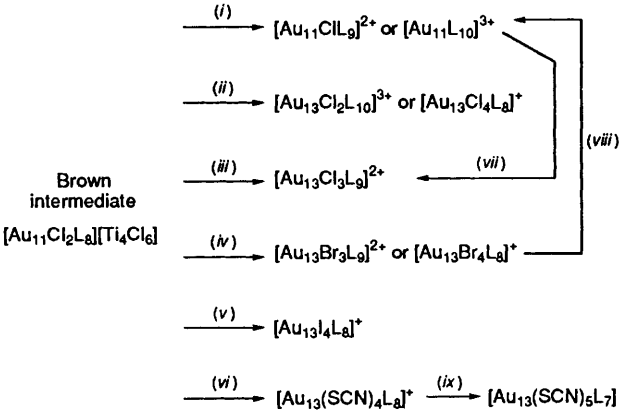

Scheme 1 The formation and reactions of Au_{13} cluster compounds containing the $PMePh_2$ phosphine ligand (L). The brown intermediate, postulated as $[Au_{11}Cl_2L_8][TiCl_4]$, is formed from the reduction of [AuCl(L)] using $[Ti(\eta\text{-}C_6H_5Me)_2]$ in toluene at reduced temperatures. (*i*) Counter anion; (*ii*) stirred in air; (*iii*) LiCl; (*iv*) LiBr; (*v*) KI; (*vi*) KSCN; (*vii*) [AuCl(L)] or Cl^-; (*viii*) L; (*ix*) SCN^-, 72 °C, 24 h. Reactions (*i*)-(*vi*), (*viii*) in alcohol, (*vii*) in CH_2Cl_2

The large discrepancy in these values, due to relativistic effects, means that the gold atoms prefer sites of high electron density and being bonded to the electron-donating phosphine groups.

The most recent development in the area of gold–silver supracluster chemistry has been the discovery of 25-metal-atom trimetallic compounds.[9] These have been prepared from smaller preformed cluster compounds. Similar to the bimetallic systems of the same nuclearity, a vertex-sharing biicosahedral geometry is observed.

The remaining compounds to contain heteronuclear M^{IB}–M^{IB} bonds are also trimetallic and contain either ten or eleven metal atoms.[20-24] Steggerda and co-workers have prepared these compounds by treating an electrophile, either $AgNO_3$ or CuCl, with preformed platinum–gold cluster compounds. The resulting clusters can be regarded as having either a toroidal $[(S^\sigma)^2(P^\sigma)^4]$ or a spherical $[(S^\sigma)^2(P^\sigma)^6]$ geometry. In the latter case a central platinum is bonded not only to the other metals

but also to a ligand of its own and the metal cage can be related to a fragment of a centred icosahedron. The heteronuclear M^{IB}–M^{IB} tangential distances tend to be shorter in the toroidal cluster compounds.

This paper describes homo- and hetero-nuclear gold cluster compounds that contain a centred icosahedral metal framework and in particular the cluster series with the general formula $[Au_9M^{IB}{}_4Cl_4(PMePh_2)_8][C_2B_9H_{12}]$, where M^{IB} = Au, Ag or Cu. This series gives an ideal opportunity to investigate the effects of introducing heteroatoms into a highly symmetrical homonuclear cage geometry.

Results and Discussion

The compounds $[Au_{13}Cl_4(PMePh_2)_8][C_2B_9H_{12}]$ **1**, $[Au_9Ag_4Cl_4(PMePh_2)_8][C_2B_9H_{12}]$ **2** and $[Au_9Cu_4Cl_4(PMePh_2)_8][C_2B_9H_{12}]$ **3**, denoted collectively as $[Au_9M^{IB}{}_4Cl_4(PMePh_2)_8][C_2B_9H_{12}]$, where M^{IB} = Au, Ag or Cu, were made from solutions of $[Au_{11}(PMePh_2)_{10}][C_2B_9H_{12}]_3$ by the addition or formation *in situ* of $[M^{IB}Cl(PMePh_2)]$ [equation (1)].

$$[Au_{11}(PMePh_2)_{10}][C_2B_9H_{12}]_3 + 4[M^{IB}Cl(PMePh_2)] \longrightarrow [Au_9M^{IB}{}_4Cl_4(PMePh_2)_8][C_2B_9H_{12}] + 2[Au(PMePh_2)_3][C_2B_9H_{12}] \quad (1)$$

The experimental procedures described in this paper result in high-yield syntheses of the new compounds **2** and **3**, with the reactions going to completion in seconds. This allows little time to probe the reaction mechanisms involved. In this respect, the reaction of $[Au_{11}(PMePh_2)_{10}]^{3+}$ with a large excess of Cu^ICl in CH_2Cl_2 was more interesting. The conversion into $[Au_9Cu_4Cl_4(PMePh_2)_8]^+$ took place over a period of days and was followed by ^{31}P-$\{^1H\}$ NMR spectroscopy.[25] Over this period resonances for two intermediates, thought to be $[Au_{11}Cu_2Cl_2(PMePh_2)_{10}]^{3+}$ and $[Au_{10}Cu_3Cl_3(PMePh_2)_9]^{2+}$, developed and collapsed. The existence of all the cations at the same time suggests a series of equilibrium steps, with similar equilibrium constants. The cluster compound $[Au_{11}(PMePh_2)_{10}]^{3+}$ has been shown to contain twelve peripheral Au–Au bonds in the solid state.[26] The proposed centred gold–copper icosahedral clusters contain a further two radial and eighteen tangential bonds and the formation of these is believed to drive the reaction yielding $[Au_{11}Cu_2Cl_2(PMePh_2)_{10}]^{3+}$. The subsequent conversion into $[Au_{10}Cu_3Cl_3(PMePh_2)_9]^{2+}$ and $[Au_9Cu_4Cl_4(PMePh_2)_8]^+$ reduces the non-bonded contacts between the phosphine groups and also gives the stable $[Au(PMePh_2)_3]^+$ as a by-product. Efforts to isolate $[Au_{11}Cu_2Cl_2(PMePh_2)_{10}]^{3+}$ and $[Au_{10}Cu_3Cl_3(PMePh_2)_9]^{2+}$ in a pure form were unsuccessful, with further interconversions taking place during recrystallization. Aware of the existence of the intermediates, similar cations could be recognized by their NMR resonances when low stoichiometric ratios of $[AuCl(PMePh_2)]$ or $[AgCl(PMePh_2)]$ were added to solutions of $[Au_{11}(PMePh_2)_{10}]^{3+}$. As before, however, isolation of the cations proved impossible.

Crystal structure of cluster $2{\cdot}H_2O{\cdot}0.5CH_2Cl_2$

The structure determination of $2{\cdot}H_2O{\cdot}0.5CH_2Cl_2$ was described in a preliminary communication[27] and fractional atomic coordinates have been deposited with the Cambridge Crystallographic Data Centre. For the purposes of the following discussion, selected interatomic distances are given in Table 1. A perspective drawing of the inner co-ordination sphere of the $[Au_9Ag_4Cl_4(PMePh_2)_8]^+$ cation is shown in Fig. 1. The metal cage geometry closely resembles that of the isoelectronic $[Au_{13}Cl_2(PMe_2Ph)_{10}]^{3+}$. Although no crystallographic symmetry is imposed on the cation the framework has idealized C_{2v} symmetry. There is no evidence to suggest that

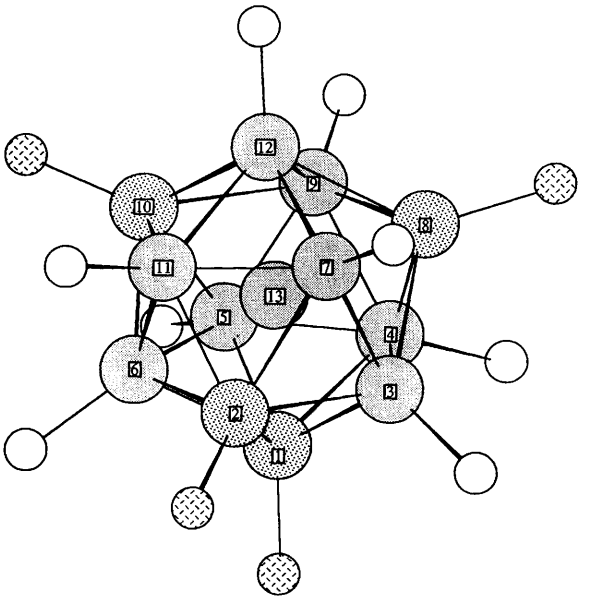

Fig. 1 Perspective view of the $[Au_9Ag_4Cl_4(PMePh_2)_8]^+$ cluster cation. Phosphine substituents and bonds to the central atom are omitted for clarity. Key to atom type patterns: gold, fine speckling; silver, course speckling; phosphorus, no pattern; chlorine, herringbone. The metal atoms are labelled with their serial numbers

the metal sites are disordered and the position of highest connectivity is occupied by a gold atom. This is in line with site-preference considerations derived theoretically.[28] With the exception of the interstitial atom, each metal is associated with one terminal ligand. As in the gold–silver supraclusters, the phosphine and halide ligands are associated with the gold and silver atoms respectively.

The Au–Au radial distances found in compound $2{\cdot}H_2O{\cdot}0.5CH_2Cl_2$ have a narrow range of values, the mean of which is 2.746 ± 0.013 Å.* This average lies between the 2.713 ± 0.019 and the 2.779 ± 0.008 Å reported for $[Au_{13}Ag_{12}Cl_7\{P(C_6H_4Me\text{-}p)_3\}_{10}]^{2+}$ (ref. 8) and $[Au_{13}Cl_2(PMe_2Ph)_{10}]^{3+}$ respectively.†[2] The former cation has been chosen as a representative example of the Teo gold–silver supraclusters for the purposes of this discussion. The radial distances to the silver atoms in the $[Au_9Ag_4Cl_4(PMePh_2)_8]^+$ cation also fall within a small range but the mean distance of 2.828 ± 0.018 Å is significantly longer than that just discussed for the gold atoms. Whilst the two metals do not bear identical ligands it is unlikely that this is the cause of the difference: in $[Au_{13}Cl_2(PMe_2Ph)_{10}]^{3+}$ the peripheral metals bonded to a halide ligand are associated with the shortest radial distances. Since gold and silver have identical metallic radii[29] the implication is that the heteronuclear bonding interactions are weaker. A similar difference in radial distances is seen in $[Au_{13}Ag_{12}Cl_7$-

* The sample standard deviation is provided after all mean values in this paper and is defined as $\sigma_{n-1} = [\{\Sigma x^2 - [(\Sigma x)^2/n]\}/(n-1)]^{\frac{1}{2}}$ where: σ_{n-1} = sample standard deviation, Σx^2 = sum of the squared observations, $(\Sigma x)^2$ = sum of the observations squared and n = number of observations.

† In the discussion several references are made to the cluster compounds $[Au_{13}Ag_{12}Cl_7\{P(C_6H_4Me\text{-}p)_3\}_{10}][SbF_6]_2$ and $[Au_{13}Cl_2(PMe_2Ph)_{10}][PF_6]_3$. The two outer icosahedra in the former are identical as a result of a crystallographic two-fold axis. For comparative purposes, only distances within a centred *nido* Au_6Ag_6 fragment are considered because the shared vertex, whilst peripheral to the outer icosahedra, is clearly also interstitial. The cage in $[Au_{13}Cl_2(PMe_2Ph)_{10}][PF_6]_3$ contains gold atoms that are bonded to halide ligands. Since this is not the case for $2{\cdot}H_2O{\cdot}0.5CH_2Cl_2$ and because these distances are somewhat atypical for the cluster as a whole, bond lengths to the Au–Cl moieties are excluded from the analysis.

Table 1 Selected interatomic distances (Å) for the cations of clusters **2**·H_2O·0.5CH_2Cl_2 and **3**·CH_2Cl_2

2·H_2O·0.5CH_2Cl_2		**3**·CH_2Cl_2	
Radial cage			
Ag(1)–Au(13)	2.814(2)	Cu(1)–Au(13)	2.602(2)
Ag(2)–Au(13)	2.853(2)	Cu(2)–Au(13)	2.605(2)
Ag(8)–Au(13)	2.830(2)	Cu(8)–Au(13)	2.564(2)
Ag(10)–Au(13)	2.815(2)	Cu(10)–Au(13)	2.565(2)
Range 2.814(2)–2.853(2), mean 2.828 ± 0.018		2.564(2)–2.605(2), 2.584 ± 0.023	
Au(3)–Au(13)	2.743(1)	Au(3)–Au(13)	2.754(1)
Au(4)–Au(13)	2.752(1)	Au(4)–Au(13)	2.724(1)
Au(5)–Au(13)	2.750(1)	Au(5)–Au(13)	2.748(1)
Au(6)–Au(13)	2.756(1)	Au(6)–Au(13)	2.746(1)
Au(7)–Au(13)	2.767(1)	Au(7)–Au(13)	2.727(1)
Au(9)–Au(13)	2.734(1)	Au(9)–Au(13)	2.728(1)
Au(11)–Au(13)	2.742(1)	Au(11)–Au(13)	2.727(1)
Au(12)–Au(13)	2.725(1)	Au(12)–Au(13)	2.744(1)
Range 2.725(1)–2.767(1), mean 2.746 ± 0.013		2.724(1)–2.754(1), 2.737 ± 0.012	
Tangential cage			
Ag(1)–Ag(2)	2.946(2)	Cu(1)–Cu(2)	2.677(3)
Ag(1)–Au(3)	2.895(2)	Cu(1)–Au(3)	2.731(2)
Ag(1)–Au(4)	2.873(2)	Cu(1)–Au(4)	2.748(2)
Ag(1)–Au(5)	2.945(2)	Cu(1)–Au(5)	2.849(2)
Ag(1)–Au(6)	2.846(2)	Cu(1)–Au(6)	2.706(2)
Ag(2)–Au(3)	2.814(2)	Cu(2)–Au(3)	2.745(2)
Ag(2)–Au(6)	2.908(2)	Cu(2)–Au(6)	2.715(2)
Ag(2)–Au(7)	3.078(2)	Cu(2)–Au(7)	2.745(2)
Ag(2)–Au(11)	2.835(2)	Cu(2)–Au(11)	2.871(2)
Au(3)–Ag(8)	2.964(2)	Au(3)–Cu(8)	2.783(2)
Au(4)–Ag(8)	2.880(2)	Au(4)–Cu(8)	2.874(2)
Au(5)–Ag(10)	2.924(2)	Au(5)–Cu(10)	2.709(2)
Au(6)–Ag(10)	2.891(2)	Au(6)–Cu(10)	2.862(2)
Au(7)–Ag(8)	2.875(2)	Au(7)–Cu(8)	2.745(2)
Ag(8)–Au(9)	2.918(2)	Cu(8)–Au(9)	2.814(2)
Ag(8)–Au(12)	3.072(2)	Cu(8)–Au(12)	2.810(2)
Au(9)–Ag(10)	3.055(2)	Au(9)–Cu(10)	2.906(2)
Ag(10)–Au(11)	2.963(2)	Cu(10)–Au(11)	2.748(3)
Ag(10)–Au(12)	2.895(2)	Cu(10)–Au(12)	2.866(2)
Range 2.814(2)–3.078(2), mean 2.924 ± 0.078		2.706(2)–2.906(2), 2.790 ± 0.066	
Au(3)–Au(4)	2.916(1)	Au(3)–Au(4)	2.848(1)
Au(3)–Au(7)	2.861(1)	Au(3)–Au(7)	2.897(1)
Au(4)–Au(5)	2.931(1)	Au(4)–Au(5)	2.913(1)
Au(4)–Au(9)	2.951(1)	Au(4)–Au(9)	2.873(1)
Au(5)–Au(6)	2.889(1)	Au(5)–Au(6)	2.890(1)
Au(5)–Au(9)	2.886(1)	Au(5)–Au(9)	2.956(1)
Au(6)–Au(11)	2.925(1)	Au(6)–Au(11)	2.883(1)
Au(7)–Au(11)	2.904(1)	Au(7)–Au(11)	2.905(1)
Au(7)–Au(12)	2.888(1)	Au(7)–Au(12)	2.962(1)
Au(9)–Au(12)	2.855(1)	Au(9)–Au(12)	2.850(1)
Au(11)–Au(12)	2.935(1)	Au(11)–Au(12)	2.913(1)
Range 2.855(1)–2.951(1), mean 2.904 ± 0.031		2.848(1)–2.962(1), 2.899 ± 0.037	
Metal–ligand			
Ag(1)–Cl(1)	2.368(6)	Cu(1)–Cl(1)	2.121(5)
Ag(2)–Cl(2)	2.381(6)	Cu(2)–Cl(2)	2.131(6)
Ag(8)–Cl(8)	2.385(6)	Cu(8)–Cl(8)	2.151(5)
Ag(10)–Cl(10)	2.377(6)	Cu(10)–Cl(10)	2.134(6)
Range 2.368(6)–2.385(6), mean 2.378 ± 0.007		2.121(5)–2.151(5), 2.134 ± 0.012	
Au(3)–P(3)	2.294(5)	Au(3)–P(3)	2.290(5)
Au(4)–P(4)	2.306(5)	Au(4)–P(4)	2.281(5)
Au(5)–P(5)	2.297(5)	Au(5)–P(5)	2.306(5)
Au(6)–P(6)	2.297(6)	Au(6)–P(6)	2.280(5)
Au(7)–P(7)	2.306(5)	Au(7)–P(7)	2.300(5)
Au(9)–P(9)	2.297(5)	Au(9)–P(9)	2.284(5)
Au(11)–P(11)	2.300(5)	Au(11)–P(11)	2.299(5)*
—		Au(11)–P(21)	2.303(5)*
Au(12)–P(12)	2.293(5)	Au(12)–P(12)	2.287(5)
Range 2.293(5)–2.306(5), mean 2.299 ± 0.005		2.280(5)–2.306(5), 2.290 (± 0.010)	

* Subject to restraints and not included in the mean calculation.

$\{P(C_6H_4Me\text{-}p)_3\}_{10}]^{2+}$, where the slightly shorter mean of 2.804 ± 0.048 Å is observed for the Au–Ag bonds.

In common with homonuclear gold cluster compounds, the tangential cage bond lengths discovered in $2\cdot H_2O\cdot 0.5CH_2Cl_2$ are longer and vary more than the radial ones. The mean tangential distances can be ordered, Au–Au < Au–Ag < Ag–Ag, although the significance of this is somewhat limited, given the range of values seen in the first two cases and given that only one Ag–Ag contact exists. The peripheral Au–Au distances in the $[Au_9Ag_4Cl_4(PMePh_2)_8]^+$ cation have a mean of 2.904 ± 0.031 Å. This figure is very close to the value of 2.919 ± 0.024 Å found for $[Au_{13}Cl_2(PMe_2Ph)_{10}]^{3+}$. In conjunction with the figures discussed for radial Au–Au bond lengths, it would seem that the addition of the heteroatoms into the cage has had little effect on the homonuclear separations. The Au–Ag peripheral contacts have an average length of 2.924 ± 0.078 Å. This mean lies between that for the compounds $[Pt(CO)(AgNO_3)(AuPPh_3)_8][NO_3]_2$ and $[Pt(PPh_3)(AgNO_3)_3(AuPPh_3)_6]$.[22,24] Compared to $[Au_{13}Ag_{12}Cl_7\{P(C_6H_4Me\text{-}p)_3\}_{10}]^{2+}$, the range of Au–Ag distances is somewhat larger in $2\cdot H_2O\cdot 0.5CH_2Cl_2$ but the means are within 0.01 Å of one another. At 2.946(2) Å the Ag–Ag bond length in the $[Au_9Ag_4Cl_4(PMePh_2)_8]^+$ cation is well within the range of distances reported for $[Au_{13}Ag_{12}Cl_7\{P(C_6H_4Me\text{-}p)_3\}_{10}]^{2+}$ and somewhat longer than the 2.889 Å found for the bulk metal.[30]

In the $[Au_9Ag_4Cl_4(PMePh_2)_8]^+$ cation the angles at the peripheral metals between the co-ordinating atom of each ligand and Au(13) range between 166.3(2) and 179.4(2)°, giving a mean of 172.7 ± 4.0°. The deviation from linearity is similar to that in $[Au_{13}Cl_2(PMe_2Ph)_{10}]^{3+}$. Considering cluster cone angles,[31] the mean value for $[Au_{13}Cl_4(PMePh_2)_8]^+$ is 6° greater than that for $[Au_{13}Cl_2(PMe_2Ph)_{10}]^{3+}$. Assuming $[Au_9Ag_4Cl_4(PMePh_2)_8]^+$ and $[Au_{13}Cl_4(PMePh_2)_8]^+$ to merit similar mean cone angles, it is perhaps surprising that deviations from linearity are not greater in $2\cdot H_2O\cdot 0.5CH_2Cl_2$. This is probably because the additional halide ligands allow the bulkier phosphines to pack more efficiently. Summarizing the ligand arrangement for the cation of $2\cdot H_2O\cdot 0.5CH_2Cl_2$, the deviations from linearity ease steric pressure, with a general trend of the phosphine groups moving towards the more open regions, nearer the halide ligands.

Crystal structure of cluster $3\cdot CH_2Cl_2$

Fractional atomic coordinates for cluster $3\cdot CH_2Cl_2$ are listed in Table 2, with a full description of the numbering scheme given in the Experimental section. The metal cage is once again a centred icosahedron and the copper atoms are positioned identically to the silver atoms in the $[Au_9Ag_4Cl_4(PMePh_2)_8]^+$ cation. Whilst the cation is generally well ordered, the phosphine group associated with Au(11) was modelled in two orientations, as a major and a minor component. There are four different ways the metal cages and ligands of $2\cdot H_2O\cdot 0.5CH_2Cl_2$ and $3\cdot CH_2Cl_2$ can be compared. Disregarding the disorder in the region of Au(11) for $3\cdot CH_2Cl_2$, the ligand arrangements for the two cations cannot be superimposed. For this reason no attempt is made to compare individual bond lengths in the discussion below. Clusters $2\cdot H_2O\cdot 0.5CH_2Cl_2$ and $3\cdot CH_2Cl_2$ crystallize in the same space group but the unit cells cannot be transformed into one another. It is interesting that whilst a full structure determination has never been carried out on a homonuclear $[Au_{13}X_4(PMePh_2)_8]^+$ cluster compound, where X = Cl, Br or I, a preliminary study was undertaken on $[Au_{13}Br_4(PMePh_2)_8]Br$.[4] The crystal system also appeared to be monoclinic, with similar unit-cell parameters to those for $3\cdot CH_2Cl_2$.

Selected interatomic distances for cluster $3\cdot CH_2Cl_2$ are given in Table 1. The mean radial Au–Au distance is 2.737 ± 0.012 Å and is very similar to the 2.746 ± 0.013 Å found in the cation of $2\cdot H_2O\cdot 0.5CH_2Cl_2$. At 2.584 ± 0.023 Å the mean radial Au–Cu distance is far shorter than the Au–Au separation and accurately reflects the 0.15 Å difference in the metallic radii of gold and copper.[29]

As with the radial bonds, the ranges and means for the tangential Au–Au bonds in $[Au_9Ag_4Cl_4(PMePh_2)_8]^+$ and $[Au_9Cu_4Cl_4(PMePh_2)_8]^+$ are very similar. Once again, homonuclear separations appear to have been little affected by the presence of the heteroatoms. For $3\cdot CH_2Cl_2$ this is perhaps more surprising, given the distortions that might have been expected on the basis of introducing the first-row transition metal. The heteronuclear tangential contacts in $3\cdot CH_2Cl_2$ are far shorter than in $2\cdot H_2O\cdot 0.5CH_2Cl_2$, although there is some overlap in the ranges observed for both cluster cations. The mean peripheral Au–Cu length is 2.790 ± 0.066 Å and is somewhat shorter than the 2.826 ± 0.123 Å reported for $[Pt(CO)(CuCl)(AuPPh_3)_8][NO_3]_2$.[24] The equivalent distance for $[Pt(CuCl)(AuPPh_3)_8][NO_3]_2$ was 2.661 ± 0.028 Å,[20] where the low value reflects the toroidal topology of the cluster. The single Cu–Cu bond length is 2.677(3) Å and is significantly longer than the interatomic separation of 2.556 Å reported for elemental copper.[30]

Comparing the cation found in cluster $3\cdot CH_2Cl_2$ to that in $2\cdot H_2O\cdot 0.5CH_2Cl_2$, the Au–Au bond lengths have been shown to be very similar but there are large differences between the Au–Cu and the Au–Ag bond lengths. To achieve this the Cu–Cl and Ag–Cl moieties can be visualized as moving relative to one another along radial vectors.

In considering the ligand packing around the cation in cluster $3\cdot CH_2Cl_2$ some effort was made to identify any disorder in the phosphine groups surrounding Au(11). None could be identified, although higher than expected isotropic displacement parameters are associated with one of the phenyl rings indirectly bound to Au(6). Disregarding the disordered phosphine position, the angles from the centre of the cage to the ligands *via* the peripheral metals range from 167.8(1) to 179.1(2)° and give a mean of 174.1 ± 3.8°. The angles to the two disordered components at Au(11) are 168.0(2) and 164.8(3)°. These large deviations from linearity may be affected by the model chosen but alternatively might help to explain the instability seen in the region of Au(11). Once again there is a trend of phosphine groups leaning towards the sterically less challenged regions close to the heteroatoms.

Spectroscopic characterization of $[Au_9M^{IB}{}_4Cl_4(PMePh_2)_8][C_2B_9H_{12}]$

For many years the UV/VIS spectra of gold cluster compounds were loosely explained in terms of electronic transitions within the metal framework. Recently, attempts have been made to interpret spectra in terms of specific skeletal geometries and the molecular orbitals associated with these.[32]

The electronic spectra of the cluster compounds under investigation are depicted in Fig. 2. The spectrum of $[Au_{13}Cl_4(PMePh_2)_8]^+$ is very similar to that of $[Au_{13}Cl_2(PMe_2Ph)_{10}]^{3+}$:[1] it is a general finding in gold cluster chemistry that the spectra are highly dependent on the cage nuclearity but far less so on the associated ligands.[1] The spectrum of $[Au_9Ag_4Cl_4(PMePh_2)_8]^+$ contains many of the features seen for $[Au_{13}Cl_4(PMePh_2)_8]^+$. The largest peak is broader than in the homonuclear case and blue shifted by 17 nm but the absorption coefficient is very similar. Teo *et al.*[33] have noted that the effect of increasing the proportion of silver in mixed gold–silver colloids is to cause a similar blue shift in the electronic spectrum. The spectrum of $[Au_{18}Ag_{20}Cl_{14}(PPh_3)_{12}]$ is very similar to that for $[Au_9Ag_4Cl_4(PMePh_2)_8]^+$ but the dominant feature is shifted to 495 nm.[33] Compared to $[Au_9Ag_4Cl_4(PMePh_2)_8]^+$, $[Au_9Cu_4Cl_4(PMePh_2)_8]^+$ has a UV/VIS spectrum which is further removed from that of the

Table 2 Fractional atomic coordinates for cluster **3**·CH_2Cl_2

Atom	*x*	*y*	*z*
Cu(1)	0.184 6(1)	0.785 48(8)	0.342 9(1)
Cu(2)	0.236 8(1)	0.768 36(9)	0.239 3(1)
Au(3)	0.256 96(3)	0.699 88(3)	0.340 15(3)
Au(4)	0.147 38(3)	0.692 54(3)	0.390 41(3)
Au(5)	0.060 78(3)	0.761 34(3)	0.316 50(3)
Au(6)	0.126 65(3)	0.812 42(3)	0.226 82(3)
Au(7)	0.237 09(4)	0.663 25(3)	0.209 50(3)
Cu(8)	0.180 3(1)	0.616 85(8)	0.301 0(1)
Au(9)	0.060 06(3)	0.646 43(3)	0.294 81(3)
Cu(10)	0.047 6(1)	0.725 64(9)	0.195 0(1)
Au(11)	0.148 82(4)	0.731 43(3)	0.138 01(3)
Au(12)	0.110 97(3)	0.629 72(3)	0.181 19(3)
Au(13)	0.148 54(3)	0.709 92(3)	0.263 89(3)
Cl(1)	0.215 9(3)	0.847 8(2)	0.405 3(3)
Cl(2)	0.308 4(3)	0.816 2(2)	0.217 6(3)
P(3)	0.343 2(2)	0.699 2(2)	0.411 1(2)
P(4)	0.143 4(2)	0.681 3(2)	0.496 4(2)
P(5)	−0.016 5(2)	0.812 5(2)	0.341 7(3)
P(6)	0.129 0(2)	0.900 3(2)	0.205 6(3)
P(7)	0.317 0(2)	0.621 3(2)	0.176 2(2)
Cl(8)	0.215 7(2)	0.540 7(2)	0.330 1(2)
P(9)	−0.016 2(2)	0.593 0(2)	0.314 6(2)
Cl(10)	−0.036 5(3)	0.747 3(3)	0.143 0(3)
P(12)	0.072 0(2)	0.567 6(2)	0.109 0(2)
P(11)	0.128 4(4)	0.753 9(3)	0.032 2(2)
P(21)	0.172 6(5)	0.737 7(5)	0.036 3(3)
C(311)	0.348 3(7)	0.650 8(5)	0.475 3(6)
C(312)	0.388 0(6)	0.657 4(5)	0.531 4(7)
C(313)	0.388 7(6)	0.621 3(6)	0.581 0(6)
C(314)	0.349 6(8)	0.578 6(6)	0.574 4(7)
C(315)	0.309 9(7)	0.572 1(5)	0.518 2(8)
C(316)	0.309 3(6)	0.608 2(6)	0.468 7(6)
C(321)	0.407 2(6)	0.689 9(6)	0.372 1(7)
C(322)	0.444 8(7)	0.646 8(6)	0.386 6(7)
C(323)	0.493 5(7)	0.639 3(6)	0.354 3(9)
C(324)	0.504 6(7)	0.674 9(8)	0.307 4(8)
C(325)	0.467 0(8)	0.718 0(7)	0.292 9(7)
C(326)	0.418 3(7)	0.725 5(5)	0.325 3(8)
C(331)	0.353(1)	0.762 2(9)	0.450(1)
C(411)	0.147 7(6)	0.612 6(4)	0.521 4(6)
C(412)	0.143 0(6)	0.599 2(5)	0.584 2(5)
C(413)	0.144 5(7)	0.546 5(5)	0.602 5(5)
C(414)	0.150 8(7)	0.507 3(4)	0.558 0(7)
C(415)	0.155 5(7)	0.520 7(4)	0.495 3(6)
C(416)	0.154 0(6)	0.573 4(5)	0.477 0(4)
C(421)	0.200 3(6)	0.716 2(6)	0.547 1(7)
C(422)	0.245 8(7)	0.691 3(4)	0.587 5(8)
C(423)	0.289 9(6)	0.721 1(6)	0.624 0(7)
C(424)	0.288 5(7)	0.775 8(6)	0.620 0(8)
C(425)	0.242 9(8)	0.800 7(4)	0.579 6(9)
C(426)	0.198 9(6)	0.770 9(6)	0.543 1(7)
C(431)	0.072 9(9)	0.705 2(8)	0.517(1)
C(511)	0.002 0(7)	0.855 9(5)	0.409 3(6)
C(512)	0.059 1(6)	0.852 2(5)	0.443 8(7)
C(513)	0.075 6(5)	0.884 7(7)	0.496 3(7)
C(514)	0.035 0(8)	0.921 0(6)	0.514 2(7)
C(515)	−0.022 1(7)	0.924 7(6)	0.479 7(8)
C(516)	−0.038 6(5)	0.892 1(6)	0.427 2(7)
C(521)	−0.083 6(5)	0.778 7(6)	0.355 2(7)
C(522)	−0.104 7(7)	0.777 4(6)	0.413 7(6)
C(523)	−0.158 9(7)	0.753 1(7)	0.418 8(6)
C(524)	−0.192 1(6)	0.730 1(7)	0.365 3(8)
C(525)	−0.171 0(7)	0.731 4(6)	0.306 8(7)
C(526)	−0.116 7(7)	0.755 7(6)	0.301 8(6)
C(531)	−0.041(1)	0.855 0(9)	0.277(1)
C(611)	0.085 9(6)	0.941 6(5)	0.251 0(6)
C(612)	0.038 4(6)	0.972 5(6)	0.223 1(5)
C(613)	0.006 7(6)	1.003 1(6)	0.261 2(7)
C(614)	0.022 6(7)	1.002 8(6)	0.327 2(7)
C(615)	0.070 1(7)	0.971 9(6)	0.355 1(5)
C(616)	0.101 8(6)	0.941 3(6)	0.317 0(7)
C(621)	0.105 6(9)	0.918 6(8)	0.123 6(8)
C(622)	0.125 1(8)	0.963 8(8)	0.096(1)
C(623)	0.101(1)	0.977 7(7)	0.034(1)
C(624)	0.056(1)	0.946(1)	−0.000 1(8)
C(625)	0.036 9(9)	0.901 1(9)	0.028(1)
C(626)	0.061 5(9)	0.887 2(7)	0.090(1)
C(631)	0.203(1)	0.925 7(9)	0.221(1)
C(711)	0.298 7(6)	0.571 5(5)	0.116 2(6)
C(712)	0.320 5(6)	0.571 8(5)	−0.058 1(7)
C(713)	0.307 3(7)	0.530 3(6)	0.015 4(5)
C(714)	0.272 2(7)	0.488 5(5)	0.030 9(6)
C(715)	0.250 4(6)	0.488 2(5)	0.089 1(7)
C(716)	0.263 6(6)	0.529 7(6)	0.131 7(5)
C(721)	0.369 8(7)	0.664 3(7)	0.147 0(8)
C(722)	0.426 3(8)	0.645 4(6)	0.140 3(9)
C(723)	0.467 3(6)	0.678 2(8)	0.117(1)
C(724)	0.451 8(8)	0.730 0(7)	0.100 0(9)
C(725)	0.395(1)	0.748 9(5)	0.106 7(9)
C(726)	0.354 3(7)	0.716 0(7)	0.130 3(9)
C(731)	0.358(1)	0.586 4(8)	0.243(1)
C(911)	−0.034 5(7)	0.598 1(6)	0.395 5(5)
C(912)	−0.002 2(6)	0.569 1(5)	0.444 7(7)
C(913)	−0.014 8(6)	0.574 2(6)	0.506 8(6)
C(914)	−0.059 7(7)	0.608 3(6)	0.519 7(5)
C(915)	−0.091 9(6)	0.637 3(6)	0.470 6(7)
C(916)	−0.079 3(6)	0.632 2(6)	0.408 5(6)
C(921)	−0.001 6(7)	0.523 6(5)	0.305 3(8)
C(922)	0.056 1(6)	0.505 3(6)	0.325 1(7)
C(923)	0.069 0(6)	0.452 0(6)	0.320 4(8)
C(924)	0.024 1(8)	0.416 9(5)	0.296 0(9)
C(925)	−0.033 6(7)	0.435 2(6)	0.276 3(9)
C(926)	−0.046 5(5)	0.488 5(7)	0.280 9(8)
C(931)	−0.082(1)	0.609(1)	0.263(1)
C(1111)	0.172(1)	0.809 4(9)	0.013(2)
C(1112)	0.218(2)	0.828(1)	0.059(1)
C(1113)	0.255(1)	0.869(1)	0.045(2)
C(1114)	0.246(1)	0.891(1)	−0.016(2)
C(1115)	0.201(2)	0.873(1)	−0.062(1)
C(1116)	0.164(1)	0.832(1)	−0.048(2)
C(1121)	0.141(1)	0.704(1)	−0.025(1)
C(1122)	0.196(1)	0.679(1)	−0.016(1)
C(1123)	0.209(1)	0.641(1)	−0.059(2)
C(1124)	0.166(2)	0.628(1)	−0.111(1)
C(1125)	0.111(1)	0.653(1)	−0.120(1)
C(1126)	0.098(1)	0.691(1)	−0.077(1)
C(1131)	0.052 8(8)	0.774(1)	0.007(2)
C(1211)	0.094 9(6)	0.500 0(4)	0.124 2(6)
C(1212)	0.084 4(6)	0.461 8(5)	0.076 7(4)
C(1213)	0.104 3(6)	0.410 4(4)	0.089 1(6)
C(1214)	0.134 7(6)	0.397 2(4)	0.148 9(6)
C(1215)	0.145 2(6)	0.435 4(5)	0.196 4(5)
C(1216)	0.125 3(6)	0.486 8(4)	0.184 0(5)
C(1221)	−0.009 2(5)	0.566 3(6)	0.102 0(7)
C(1222)	−0.038 1(6)	0.613 7(5)	0.085 0(7)
C(1223)	−0.100 2(6)	0.616 4(5)	0.078 0(8)
C(1224)	−0.133 3(5)	0.571 8(6)	0.087 9(8)
C(1225)	−0.104 4(6)	0.524 4(5)	0.104 9(8)
C(1226)	−0.042 4(7)	0.521 6(4)	0.111 9(7)
C(1231)	0.087(1)	0.580 9(9)	0.028(1)
C(2111)	0.193(2)	0.802 6(9)	0.013(2)
C(2112)	0.226(2)	0.838(2)	0.056(2)
C(2113)	0.241(2)	0.887(1)	0.035(2)
C(2114)	0.223(2)	0.902(1)	−0.029(3)
C(2115)	0.190(3)	0.867(2)	−0.071(2)
C(2116)	0.175(2)	0.817(1)	−0.051(2)
C(2121)	0.112(1)	0.716(2)	−0.023(2)
C(2122)	0.120(1)	0.691(2)	−0.079(2)
C(2123)	0.071(2)	0.674(2)	−0.121(1)
C(2124)	0.013(1)	0.682(2)	−0.107(2)
C(2125)	0.005(1)	0.708(2)	−0.050(2)
C(2126)	0.055(2)	0.725(2)	−0.008(1)
C(2131)	0.233(2)	0.696(2)	0.020(3)
B(1)	0.306(3)	0.399(2)	0.747(3)
B(2)	0.254(3)	0.444(2)	0.716(3)
B(3)	0.253(3)	0.419(2)	0.792(3)
B(4)	0.325(3)	0.411(2)	0.830(3)
B(5)	0.369(3)	0.433(2)	0.777(3)
B(6)	0.327(3)	0.455(2)	0.708(3)
B(7)	0.235(3)	0.484(2)	0.776(3)
B(8)	0.284(3)	0.466(2)	0.843(3)
B(9)	0.353(3)	0.478(2)	0.830(3)
B(10)	0.353(3)	0.502(2)	0.757(3)
B(11)	0.282(3)	0.507(2)	0.723(3)
B(12)	0.300(3)	0.523(2)	0.803(3)
C(100)	0.163 2(9)	0.726 1(9)	0.738(2)
Cl(101)	0.089 7(6)	0.717 2(6)	0.702 2(7)
Cl(102)	0.202(1)	0.665(1)	0.747(1)
Cl(103)	0.165(2)	0.777(2)	0.792(2)

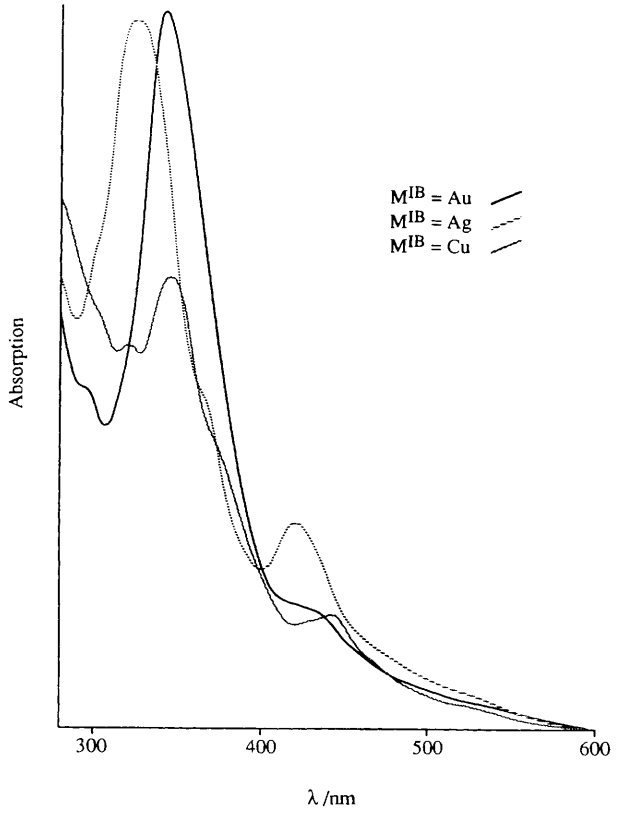

Fig. 2 Electronic spectra of the $[Au_9M^{IB}{}_4Cl_4(PMePh_2)_8][C_2B_9H_{12}]$ cluster compounds

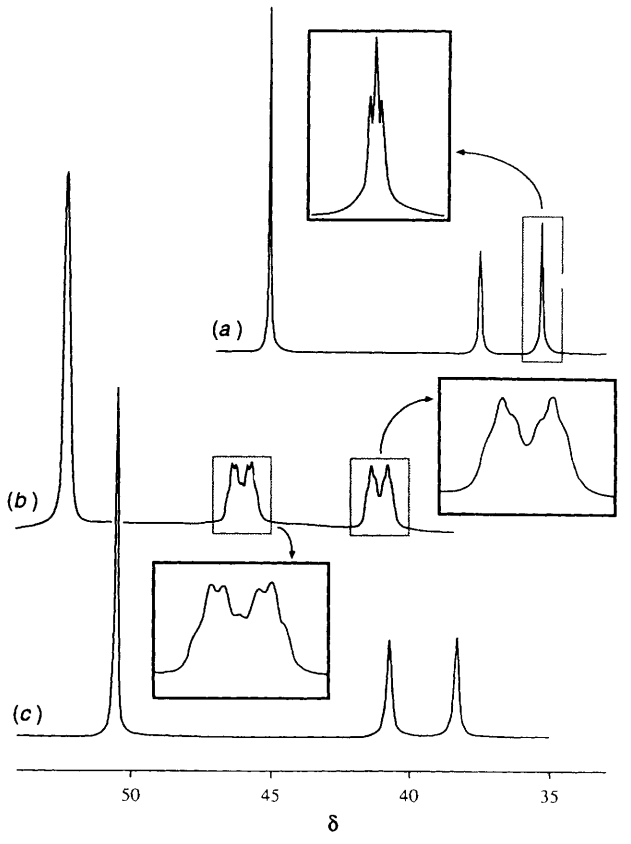

Fig. 3 The solution $^{31}P-\{^1H\}$ NMR spectra for cluster **1** (*a*), **2** (*b*) and **3** (*c*), referenced to $PO(OMe)_3$–D_2O

homonuclear member of the cluster series: the peaks have lower absorption coefficients and the largest absorption band is not as dominant.

The compounds were studied by $^{31}P-\{^1H\}$, $^{11}B-\{^1H\}$ and ^1H NMR spectroscopy. Fig. 3 shows the $^{31}P-\{^1H\}$ NMR spectra recorded for the $[Au_9M^{IB}{}_4Cl_4(PMePh_2)_8][C_2B_9H_{12}]$ cluster series. In each spectrum three signals integrate in the ratio 2:1:1, which is consistent with the solid-state structures and suggests that the icosahedral clusters are stereochemically rigid. Spin-saturation-transfer NMR studies have previously been reported as evidence for this in Au_{13} compounds.[5] The ^{31}P environments found in the $[Au_9M^{IB}{}_4Cl_4(PMePh_2)_8]^+$ cations are illustrated in Fig. 4.

The $^{31}P-\{^1H\}$ NMR spectrum for $[Au_{13}Cl_4(PMePh_2)_8]^+$ is consistent with that previously reported, with the largest resonance appearing as a singlet and associated with the four nuclei labelled as P_a in Fig. 4. The two smaller resonances are triplets. The one to high field is resolved and is found to have a coupling constant of 6 Hz. The other is unresolved. The existence of triplets can be explained in terms of ^4J(P–P) coupling, *via* the central atom, between the P_b and P_c environments shown in Fig. 4.

The $^{31}P-\{^1H\}$ NMR spectrum of $[Au_9Ag_4Cl_4(PMePh_2)_8]^+$ is the most complex. The peak to low field remains a singlet but is somewhat broader than in the spectrum of $[Au_{13}Cl_4(PMePh_2)_8]^+$. Since the arrangement of the ligands is identical to that in $[Au_{13}Cl_4(PMePh_2)_8]^+$ the ^4J(P–P) coupling previously described remains. This is not readily apparent but is thought to contribute to the shoulders seen on the two peaks to higher field. The spectrum is complicated by couplings to silver nuclei, with linewidths far larger than those seen in the homonuclear case: the half-height peak width of the singlet is 25 Hz. As a consequence there is no resolution of the individual couplings due to the ^{107}Ag and ^{109}Ag nuclei. Both of the higher-field features are split by a coupling of approximately 70 Hz and this is thought to be due to a ^3J(Ag–P) interaction, where the nuclei concerned are directly opposite one another relative to

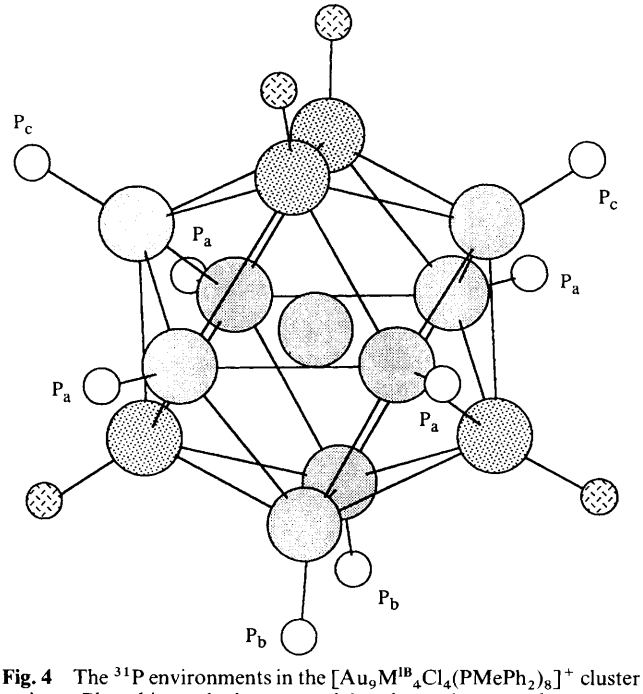

Fig. 4 The ^{31}P environments in the $[Au_9M^{IB}{}_4Cl_4(PMePh_2)_8]^+$ cluster cations. Phosphine substituents and bonds to the central atom are omitted for clarity. Key to atom type patterns: gold, fine speckling; M^{IB}, coarse speckling; phosphorus, no pattern; chlorine, herringbone

the central cage. This *para* relationship can be seen in Fig. 4 for both the P_b and P_c environments. The central resonance in the spectrum of $[Au_9Ag_4Cl_4(PMePh_2)_8]^+$, associated with P_b, contains evidence of further splitting however. This is proposed to arise from ^3J(Ag–P) coupling where the silver atom occupies a *meta* cage position relative to the ^{31}P site. Such an arrangement is not found for the environment labelled as P_c, hence the simpler higher-field feature.

The ^{31}P-{^{1}H} NMR spectrum of $[Au_9Cu_4Cl_4(PMePh_2)_8]^+$ consists of just three singlets. The simplification from the $[Au_{13}Cl_4(PMePh_2)_8]^+$ spectrum is thought to result from the presence of quadrupolar copper nuclei (^{63}Cu, spin $\frac{3}{2}$, abundance 69.1%; ^{65}Cu, spin $\frac{3}{2}$ abundance 30.9%).

The $[Au_9M^{IB}{}_4Cl_4(PMePh_2)_8]^+$ cluster cations show interesting chemical shift differences. The results are somewhat surprising since they suggest that the shielding at the ^{31}P nuclei is greatest in $[Au_{13}Cl_4(PMePh_2)_8]^+$ and least in $[Au_9Ag_4Cl_4(PMePh_2)_8]^+$. This would not be expected from the electronegativities of the M^{IB}–Cl moieties and as such it is possible that the excited-state terms for the three clusters differ.

The ^1H NMR spectra of the $[Au_9M^{IB}{}_4Cl_4(PMePh_2)_8]^+$ cations are similar to those previously described for the $[Au_{13}X_4(PMePh_2)_8]^+$ series,[4,5] where X = Cl, Br or I. Two doublets and a triplet are seen in the methyl region. The integrated intensities of the first two features are equal and half that of the third. The doublets are associated with the substituents bonded to the phosphorus atoms labelled as P_b and P_c in Fig. 4. The triplet can be associated with the methyl groups attached to the four atoms labelled P_a. The multiplet is thought to result from a virtual coupling effect,[34] with the ^1H nuclei interacting with the mutually *trans* phosphorus atoms. In the case of $[Au_9Cu_4Cl_4(PMePh_2)_8][C_2B_9H_{12}]$ the multiplets in the methyl region were not resolved and appeared as broad singlets.

The ^{11}B-{^{1}H} NMR spectra of the $[Au_9M^{IB}{}_4Cl_4(PMePh_2)_8][C_2B_9H_{12}]$ compounds were identical and consisted of five singlets with integrated intensities, from low to high field, in the ratio 2:3:2:1:1. The spectrum is very similar to that reported for $[H(dmso)_2][C_2B_9H_{12}]$[35] (dmso = dimethyl sulfoxide) and confirms the independence of the anion in solution.

Samples of clusters **1**–**3** were analysed by positive-ion FAB mass spectrometry. Well defined peaks are observed in the spectra, although a unique assignment for each is not always possible owing to the similar masses of the gold atom and the phosphine unit. The largest peak in the spectrum of **1** can be assigned to the parent cluster ion, M^+, where $M = Au_{13}Cl_4(PMePh_2)_8$. The only other major feature corresponds to the $[M - Au - Cl - PMePh_2]^+$ fragment. In contrast to this, the spectrum of **2** at $m/z > 2000$ contains eleven peaks with a relative abundance of 50% or greater. Once again, the $[M - Au - Cl - PMePh_2]^+$ fragment has been generated, in this case being associated with the largest peak. The parent cluster ion has a relative abundance of 80%. Noticeable about the spectrum is that the larger peaks are not associated with ions where silver atoms have been lost from the cage. Prominent in the fragmentation pattern are the ions with the general formula $[M - Au - Cl - nPMePh_2]^+$, where n = 1–5. The same series, with n = 1–6, is found for **3**. The spectrum of this compound once again has the parent cluster ion peak as the largest. Unlike in the case of **2**, assignments have been proposed for **3** that involve loss of the cage heteroatoms.

Experimental

Elemental analyses were performed by Mr. M. Gascoigne and his staff in the Microanalytical Department of the Inorganic Chemistry Laboratory, Oxford. Electronic spectra were recorded on a UVIKON 930 spectrophotometer using a matched pair of 1 cm quartz cells. Absorption coefficients are reported as log ε_{max}, where the units of ε are $dm^3\ mol^{-1}\ cm^{-1}$. Solution NMR spectroscopy was carried out on a Bruker AM-300 spectrometer, with proton decoupling for the ^{11}B and ^{31}P nuclei. For the latter, spectra were referenced to $PO(OMe)_3$–D_2O, which has a chemical shift of −2.4 ppm relative to 85% H_3PO_4. The positive-ion FAB mass spectra were recorded by Dr. J. A. Ballentine and his staff at the SERC Mass Spectrometry Service Centre (University College of Swansea). The spectra for **1** and **3** were recorded on a VG AutoSpec instrument, whilst for **2** a VG ZAB-E mass spectrometer was used. The samples were dissolved in CH_2Cl_2 and suspended in a matrix of 3-nitrobenzyl alcohol. Unless stated to the contrary, reactions were carried out using Schlenk-line techniques under dinitrogen using dried and degassed solvents. The compounds $AgNO_3$, KCl and $PMePh_2$ were used as supplied. Copper(I) chloride was purified using the published method.[36] The syntheses of $[AuCl(PMePh_2)]$ and $[Au_{11}(PMePh_2)_{10}][C_2B_9H_{12}]_3$ are recorded elsewhere.[26]

Syntheses

[AgCl(PMePh$_2$)]. The procedure was adapted from that reported for $[\{AgCl(PPh_3)\}_4]$.[37] Protected from light, AgCl was formed *in situ* by the reaction of $AgNO_3$ (2.79 g, 16.42 mmol) and KCl (10.0 g, 134.14 mmol) in water (20 cm^3). To this was added a solution of $PMePh_2$ (3.29 g, 16.43 mmol) in Et_2O (20 cm^3). The reaction mixture was stirred vigorously for 24 h. At the interface of the two solvents a cream coloured solid formed. Once isolated, this was recrystallized from CH_2Cl_2–EtOH to give a white microcrystalline sample of $[AgCl(PMePh_2)]$ (3.84 g, 11.18 mmol, 68%) (Found: C, 45.2; H, 3.7; Cl, 10.5. $C_{13}H_{13}AgClP$ requires C, 45.5; H, 3.8; Cl, 10.3%); δ_P[121.50 MHz, solvent CD_2Cl_2, standard $PO(OMe)_3$–D_2O] −11.95 (1 P, s).

Cluster 1. The compounds $[Au_{11}(PMePh_2)_{10}][C_2B_9H_{12}]_3$ (0.20 g, 0.044 mmol) and $[AuCl(PMePh_2)]$ (0.20 g, 0.462 mmol) were dissolved in aerated CH_2Cl_2 (50 cm^3). The reaction mixture was sealed in a quartz ampoule and left to stand, out of direct daylight, for 4 weeks. Slow diffusion of hexane into the solution yielded a red microcrystalline sample of **1** (0.11 g, 0.025 mmol, 57%) (Found: C, 28.8; H, 2.5. $C_{106}H_{116}Au_{13}B_9Cl_4P_8$ requires C, 28.7; H, 2.6%); λ_{max}/nm(CH_2Cl_2) 294 (sh), 341 (log ε 5.07) and 425 (sh); δ_H(300.14 MHz, solvent CD_2Cl_2, standard $SiMe_4$) 7.60–7.10 (80 H, m), 1.70 [6 H, d, J(PH) 10], 1.24 [12 H, t, J(PH) 4] and 1.15 [6 H, d, J(PH) 10]; δ_B[95.25 MHz, solvent CD_2Cl_2, standard BF_3·OEt_2] −11.54 (2 B, s), −17.43 (3 B, s), −22.59 (2 B, s), −33.70 (1 B, s) and −38.40 (1 B, s); δ_P[121.50 MHz, solvent CD_2Cl_2, standard $PO(OMe)_3$–D_2O] 45.37 (4 P, s), 37.71 [2 P, t, J(PP) unresolved] and 35.52 [2 P, t, J(PP) 6 Hz]; m/z 4303 [100%, M^+, where $M = Au_{13}Cl_4(PMePh_2)_8$], 4070 (7, $[M - Cl - PMePh_2]^+$ or $[M - Au - Cl]^+$), 3957 (14, no assignment), 3872 (64, $[M - Au - Cl - PMePh_2]^+$), 3436 (16, $[M - Au - 2Cl - 3PMePh_2]^+$), 3238 (6, $[M - 2Au - 2Cl - 3PMePh_2]^+$), 3003 (6, $[M - 2Au - 3Cl - 4PMePh_2]^+$), 2804 (8, $[M - 2Au - 3Cl - 5PMePh_2]^+$ or $[M - 3Au - 3Cl - 4PMePh_2]^+$) and 2570 (12, $[M - 3Au - 4Cl - 5PMePh_2]^+$).

Cluster 2. The compounds $[Au_{11}(PMePh_2)_{10}][C_2B_9H_{12}]_3$ (0.463 g, 0.101 mmol) and $[AgCl(PMePh_2)]$ (0.139 g, 0.405 mmol) were stirred in CH_2Cl_2 (10 cm^3) for 5 min. Over this period, the reaction mixture changed from red to russet. The addition of toluene gave a dark oil that was separated from the remaining solution and redissolved in CH_2Cl_2. A microcrystalline sample of **2** was obtained from a CH_2Cl_2–hexane recrystallization (0.314 g, 0.077 mmol, 76%) (Found: C, 30.7; H, 2.8; Cl, 4.2. $C_{106.5}H_{119}Ag_4Au_9B_9Cl_5OP_8$ requires* C, 30.9; H, 2.9; Cl, 4.3%); λ_{max}/nm(CH_2Cl_2) 303 (sh), 324 (log ε 5.07), 365 (sh) and 420 (4.53); δ_H(300.14 MHz, solvent CD_2Cl_2, standard $SiMe_4$) 7.55–7.15 (80 H, m), 1.81 [6 H, d, J(PH) 10], 1.28 [12 H, t, J(PH) 4] and 1.22 [6 H, d, J(PH) 10]; δ_B(95.25 MHz, solvent CD_2Cl_2, standard BF_3·OEt_2) −11.51 (2 B, s), −17.45 (3 B, s), −22.55 (2 B, s), −33.70 (1 B, s) and −38.33 (1 B, s); δ_P[121.50 MHz, solvent CD_2Cl_2, standard $PO(OMe)_3$–D_2O] 52.46 (4 P,

* A crystalline sample of $[Au_9Ag_4Cl_4(PMePh_2)_8][C_2B_9H_{12}]$·$H_2O$·$0.5CH_2Cl_2$ was used.

Table 3 Details of the X-ray crystal analyses of clusters $2{\cdot}H_2O{\cdot}0.5CH_2Cl_2$ and $3{\cdot}CH_2Cl_2$ [a]

	$2{\cdot}H_2O{\cdot}0.5CH_2Cl_2$	$3{\cdot}CH_2Cl_2$
Chemical formula	$C_{106.5}H_{119}Ag_4Au_9B_9Cl_5OP_8$	$C_{107}H_{118}Au_9B_9Cl_6Cu_4P_8$
M	4141.6	3988.8
a/Å	33.584(5)	22.679(6)
b/Å	15.161(4)	25.416(6)
c/Å	26.115(4)	21.213(6)
β/°	112.20(1)	98.27(2)
U/Å^3	12 312.0	12 100.2
D_c/Mg m^{-3}	2.234	2.190
$F(000)$	7660	7416
μ/cm^{-1}	115.3	118.2
Crystal colour and shape	Dark red plate	Orange-red prism
Crystal dimensions/mm	0.69 × 0.26 × 0.03	0.48 × 0.42 × 0.25
Scan technique	ω	ω–2θ
Scan width/°	0.8 + 0.35 tan θ	0.7 + 0.35 tan θ
Scan rate/° min^{-1}	0.8–5.0	0.6–5.0
2θ range/°	3–44	2–44
hkl Ranges	−1 to 35, −1 to 15, −27 to 25	0–23, 0–26, −22 to 22
Data: total, unique, observed with $I \geqslant 3\sigma(I)$	15 997, 15 047, 7656	15 649, 14 785, 7757
Decay (%)	0	10
Transmission	0.164–0.746	0.061–0.143
R_{int} [b]	0.0253	0.0451
Observations, parameters (ratio)	7805, 510 (15.3)	7890, 509 (15.5)
Chebyshev weighting scheme coefficients	3.35, −0.07, 2.16	16.8, −12.6, 12.6
Final R, wR and restrained S [b]	0.0408, 0.0468, 1.10	0.0397, 0.0432, 1.11

[a] Details in common: monoclinic, space group $P2_1/n$ (alt. $P2_1/c$, no. 14); $Z = 4$; absorption correction by ψ scans; least-squares refinement on F. [b] Defined in ref. 40.

s), 46.27 [2 P, dd, J(AgP) 68 and 17] and 41.29 [2 P, d, J(AgP) 70 Hz]; m/z 3948 [80%, M^+, where $M = Au_9Ag_4Cl_4(PMePh_2)_8$], 3747 (27, $[M - PMePh_2]^+$), 3711 (28, $[M - Cl - PMePh_2]^+$), 3516 (100, $[M - Au - Cl - PMePh_2]^+$), 3316 (84, $[M - Au - Cl - 2PMePh_2]^+$), 3114 (80, $[M - Au - Cl - 3PMePh_2]^+$), 3079 (38, $[M - Au - 2Cl - 3PMePh_2]^+$), 2916 (67, $[M - Au - Cl - 4PMePh_2]^+$ or $[M - 2Au - Cl - 3PMePh_2]^+$), 2877 (57, $[M - 2Cl - 5PMePh_2]^+$ or $[M - Au - 2Cl - 4PMePh_2]^+$), 2714 (15, $[M - Au - Cl - 5PMePh_2]^+$), 2678 (46, $[M - Au - 2Cl - 5PMePh_2]^+$), 2481 (69, $[M - 2Au - 2Cl - 5PMePh_2]^+$), 2444 (56, $[M - Au - 3Cl - 6PMePh_2]^+$), 2281 (63, $[M - 2Au - 2Cl - 6PMePh_2]^+$) and 2083 (57, $[M - 2Au - 2Cl - 7PMePh_2]^+$ or $[M - 3Au - 2Cl - 6PMePh_2]^+$).

Cluster 3. The compounds $[Au_{11}(PMePh_2)_{10}][C_2B_9H_{12}]_3$ (0.200 g, 0.044 mmol) and CuCl (0.087 g, 0.879 mmol) were stirred in MeCN (10 cm^3). To this was added $PMePh_2$ (0.088 g, 0.440 mmol), also dissolved in MeCN (10 cm^3). After 5 min the solution was colourless, with an orange precipitate. The latter was isolated and washed with MeCN (4 × 20 cm^3). A microcrystalline sample of **3** was obtained from a recrystallization using CH_2Cl_2–hexane (0.161 g, 0.041 mmol, 94%) (Found: C, 32.5; H, 3.0; Cl, 3.7. $C_{106}H_{116}Au_9B_9Cl_4Cu_4P_8$ requires C, 32.6; H, 3.0; Cl, 3.6%); λ_{max}/nm (CH_2Cl_2) 302 (sh), 320 (log ε 4.80), 346 (4.87), 370 (sh) and 432 (4.26); δ_H(300.14 MHz, solvent CD_2Cl_2, standard $SiMe_4$) 7.70–7.00 (80 H, m), 1.65 (6 H, br s), 1.30 (12 H, br s) and 1.14 (6 H, br s); δ_B(95.25 MHz, solvent CD_2Cl_2, standard $BF_3{\cdot}OEt_2$) −11.50 (2 B, s), −17.42 (3 B, s), −22.55 (2 B, s), −33.68 (1 B, s) and −38.35 (1 B, s); δ_P[121.50 MHz, solvent CD_2Cl_2, standard $PO(OMe)_3$–D_2O] 50.50 (4 P, s), 40.67 (2 P, s) and 38.26 (2 P, s); m/z 3769 [100%, M^+, where $M = Au_9Cu_4Cl_4(PMePh_2)_8$], 3569 (12, $[M + PMePh_2]^+$, 3372 (12, $[M - 2PMePh_2]^+$ or $[M - Au - PMePh_2]^+$), 3338 (19, $[M - Au - Cl - PMePh_2]^+$), 3172 (9, $[M - Au - 2PMePh_2]^+$), 3138 (32, $[M - Au - Cl - 2PMePh_2]^+$), 2972 (6, $[M - Au - 3PMePh_2]^+$), 2937 (18, $[M - Au - Cl - 3PMePh_2]^+$), 2737 (22, $[M - Au - Cl - 4PMePh_2]^+$, 2537 (21, $[M - Au - Cl - 5PMePh_2]^+$), 2437 (6, $[M - Au - Cu - 2Cl - 5PMePh_2]^+$), 2337 (10, $[M - Au - Cl - 6PMePh_2]^+$), 2239 (5, $[M - Au - Cu - 2Cl - 6PMePh_2]^+$ or $[M - 2Au - Cu - 2Cl - 5PMePh_2]^+$) and 2039 (6, $[M - Au - Cu - 2Cl - 7PMePh_2]^+$ or $[M - 2Au - Cu - 2Cl - 6PMePh_2]^+$).

Single-crystal structure determination of clusters $2{\cdot}H_2O{\cdot}0.5CH_2Cl_2$ and $3{\cdot}CH_2Cl_2$

Single crystals of clusters of $2{\cdot}H_2O{\cdot}0.5CH_2Cl_2$ and $3{\cdot}CH_2Cl_2$ were grown by slowly diffusing hexane into CH_2Cl_2 solutions of the compounds in sealed glass tubes (diameter 8 mm), previously treated with $SiCl_2Me_2$.[26,38] Suitable crystals for X-ray diffraction studies were mounted under a dinitrogen atmosphere in 0.5 mm Lindemann capillaries containing a small volume of CH_2Cl_2.

Intensity data were measured at 293 K on an Enraf-Nonius CAD4 diffractometer using graphite-monochromated molybdenum radiation (Mo-Kα, λ = 0.710 69 Å). A DEC MicroVAX 3300 computer was used to control the diffractometer and to carry out the subsequent steps involved with structure analysis. Crystallographic manipulations were carried out using the CRYSTALS suite of programs.[39] Crystal data and information relating to the data collections and structural refinements are given in Table 3. In both cases the structures were solved using direct methods[41] to give the metal atom positions. The models were subsequently developed using Fourier-difference syntheses. Hydrogen atoms were generated in calculated positions (C–H 0.96, B–H 1.09 Å), with appropriate occupancies and isotropic displacement parameters 1.2 times those of the associated carbon or boron atom. No attempt was made to model the *endo*-hydrogen atom of each anion.

With the atoms of the anion and cation modelled in cluster $2{\cdot}H_2O{\cdot}0.5CH_2Cl_2$, a Fourier-difference synthesis revealed three large residual peaks away from the atoms already placed. Two were accounted for by a partial-occupancy CH_2Cl_2 molecule. The remaining one proved a mystery, since it was positioned more than 2.5 Å from any other atom. With all charged species accounted for, the residual electron density was modelled as the oxygen atom of a water molecule. This might have originated from damp solvents or from the carborane starting material, that was recrystallized from water.

In the final cycle of refinement for cluster $2{\cdot}H_2O{\cdot}0.5CH_2Cl_2$

510 parameters were refined using full-matrix least-squares techniques. The gold, silver, phosphorus and chlorine atoms of the cation were refined anisotropically, with the remaining non-hydrogen atoms modelled using isotropic displacement parameters. The phenyl rings were treated as rigid groups, whilst the bond lengths in the anion [35] and CH_2Cl_2 molecule were restrained to idealized values. Vibrational restraints [39,42] along the bond directions were applied within the phenyl rings and the anion. Using a three-term Chebyshev weighting scheme a satisfactory agreement analysis was obtained.

For cluster **3**·CH_2Cl_2 a Fourier-difference synthesis suggested disorder in the region of the anion: an icosahedron of electron density suggested twelve possible sites for the eleven atoms. As a result, twelve boron atoms were placed with an occupancy of 0.916 67. A common isotropic displacement parameter was used for all the disordered atoms. The Fourier-difference map also revealed two areas where large residual electron density remained. The first of these was away from the other atoms and was modelled as a CH_2Cl_2 molecule with a rotational disorder about one of the C–Cl bonds. The second region where residual electron density appeared was close to one of the phosphine ligands. After careful consideration of the difference map a second phosphine group was placed on the relevant gold atom and the occupancies of the two ligands were refined, with corresponding atoms being assigned one displacement parameter.

The numbering scheme adopted for cluster **3**·CH_2Cl_2 included metal atoms that were given the same serial numbers as those reported for **2**·H_2O·0.5CH_2Cl_2 and shown in Fig. 1. Phosphorus and chlorine atoms associated with the cation were generally given the same serial number as the metal they were bonded to. The disordered phosphine ligand associated with Au(11) was modelled as two groups: the phosphorus atoms of the major and minor components are referred to as P(11) and P(21) respectively. The serial numbers for the $PMePh_2$ groups were assigned in an identical manner to that previously described.[26] The boron atoms of the disordered anion were numbered sequentially from B(1) and the hydrogen atoms associated with these were given the same serial number as the boron atom they were bonded to. A disordered CH_2Cl_2 molecule included C(100), Cl(101) and one of either Cl(102) or Cl(103). The two hydrogen atoms associated with the molecule in the orientation including Cl(102) were H(101) and H(102). A minor component included Cl(103), H(103) and H(104).

A three-term Chebyshev weighting scheme gave a satisfactory agreement analysis and in the final cycle of least-squares refinement for cluster **3**·CH_2Cl_2 509 parameters were refined using the full-matrix method. With the exception of the phosphorus atoms associated with the disordered phosphine ligand, all elements heavier than carbon were refined anisotropically. The phenyl groups were treated as rigid bodies with vibrational restraints along the bonds.[39,42]

With the disorder modelled, the *wR* value for cluster **3**·CH_2Cl_2 was better than that for **2**·H_2O·0.5CH_2Cl_2 but the peaks and troughs in the final Fourier-difference map were somewhat disappointing, ranging between −1.47 and +1.37 e Å^{-3}. Since the larger peaks were generally associated with the metal atoms the absorption correction was carefully reconsidered. Four different ψ scans were used for the correction and each gave a very similar and symmetrical profile. The method of Walker and Stuart [43] was tried on uncorrected, unmerged data using the best isotropic model available but the final residual electron density was not improved. As a result the original ψ-scan correction was kept in preference.

Complete atomic coordinates, thermal parameters and bond lengths and angles have been deposited at the Cambridge Crystallographic Data Centre. See Instructions for Authors, *J. Chem. Soc., Dalton Trans.*, 1996, Issue 1.

Acknowledgements

The authors are grateful to the SERC for their financial support (to R. C. B. C.), Johnson Matthey plc for the loan of gold and B. P. plc for a generous endowment to Imperial College.

References

1 K. P. Hall and D. M. P. Mingos, *Prog. Inorg. Chem.*, 1984, **32**, 237.
2 C. E. Briant, B. R. C. Theobald, J. W. White, L. K. Bell and D. M. P. Mingos, *J. Chem. Soc., Chem. Commun.*, 1981, 201.
3 D. M. P. Mingos, *J. Chem. Soc., Dalton Trans.*, 1976, 1163.
4 B. R. C. Theobald, D. Phil. Thesis, University of Oxford, 1981.
5 K. P. Hall, Part II Thesis, University of Oxford, 1981.
6 J. W. A. van der Velden, J. J. Bour, F. A. Vollenbroek, P. T. Beurskens, J. M. M. Smits and W. P. Bosman, *Recl. Trav. Chim. Pays-Bas*, 1981, **100**, 148.
7 B. K. Teo and K. Keating, *J. Am. Chem. Soc.*, 1984, **106**, 2224.
8 B. K. Teo and H. Zhang, *Inorg. Chem.*, 1991, **30**, 3115.
9 B. K. Teo, X. Shi and H. Zhang, *J. Cluster Sci.*, 1993, **4**, 471.
10 B. K. Teo and H. Zhang, *Angew. Chem., Int. Ed. Engl.*, 1992, **31**, 445.
11 B. K. Teo, X. Shi and H. Zhang, *J. Chem. Soc., Chem. Commun.*, 1992, 1195.
12 B. K. Teo, X. Shi and H. Zhang, *J. Am. Chem. Soc.*, 1991, **113**, 4329.
13 B. K. Teo, H. Zhang and X. Shi, *Inorg. Chem.*, 1990, **29**, 2083.
14 B. K. Teo, M. C. Hong, H. Zhang and D. B. Huang, *Angew. Chem., Int. Ed. Engl.*, 1987, **26**, 897.
15 B. K. Teo, M. Hong, H. Zhang, D. Huang and X. Shi, *J. Chem. Soc., Chem. Commun.*, 1988, 204.
16 B. K. Teo, M. Hong, H. Zhang, D. Huang and X. Shi, *J. Am. Chem. Soc.*, 1990, **112**, 8552.
17 B. K. Teo, X. Shi and H. Zhang, *Inorg. Chem.*, 1993, **32**, 3987.
18 B. K. Teo, X. Shi and H. Zhang, *Chem. Eng. News*, 1989, **67** (9th January), 6.
19 B. K. Teo, H. Zhang and X. Shi, *J. Am. Chem. Soc.*, 1993, **115**, 8489; *Inorg. Chem.*, 1994, **33**, 4086; T. G. G. M. Kappen, P. P. J. Schlebos, J. J. Bour, W. P. Bosman, J. M. M. Smits, P. T. Beurskens and J. J. Steggerda, *Inorg. Chem.*, 1994, **33**, 754.
20 M. F. J. Schoondergang, J. J. Bour, P. P. J. Schlebos, A. W. P. Vermeer, W. P. Bosman, J. M. M. Smits, P. T. Beurskens and J. J. Steggerda, *Inorg. Chem.*, 1991, **30**, 4704.
21 T. G. G. M. Kappen, P. P. J. Schlebos, J. J. Bour, W. P. Bosman, J. M. M. Smits, P. T. Beurskens and J. J. Steggerda, *Inorg. Chem.*, 1995, **34**, 2133.
22 R. P. F. Kanters, P. P. J. Schlebos, J. J. Bour, W. P. Bosman, J. M. M. Smits, P. T. Beurskens and J. J. Steggerda, *Inorg. Chem.*, 1990, **29**, 324.
23 T. G. G. M. Kappen, P. P. J. Schlebos, J. J. Bour, W. P. Bosman, G. Beurskens, J. M. M. Smits, P. T. Beurskens and J. J. Steggerda, *Inorg. Chem.*, 1995, **34**, 2121.
24 M. F. J. Schoondergang, Ph. D. Thesis, University of Nijmegen, 1992.
25 R. C. B. Copley, D. Phil. Thesis, University of Oxford, 1993.
26 R. C. B. Copley and D. M. P. Mingos, preceding paper.
27 R. C. B. Copley and D. M. P. Mingos, *J. Chem. Soc., Dalton Trans.*, 1992, 1755.
28 Z. Lin and D. M. P. Mingos, *Comments Inorg. Chem.*, 1989, **9**, 95.
29 *International Tables for Crystallography*, ed. A. J. C. Wilson, Kluwer Academic Publishers, Dordrecht, 1992, vol. C, p. 681.
30 *CRC Handbook of Chemistry and Physics*, 66th edn., ed. R. C. Weast, CRC Press, Boca Raton, FL, 1986.
31 D. M. P. Mingos, *Inorg. Chem.*, 1982, **21**, 464.
32 H. R. C. Jaw and W. R. Mason, *Inorg. Chem.*, 1991, **30**, 275, 3552.
33 B. K. Teo, K. Keating and Y.-H. Kao, *J. Am. Chem. Soc.*, 1987, **109**, 3494.
34 R. K. Harris, *Inorg. Chem.*, 1966, **5**, 701.
35 J. Buchanan, E. J. M. Hamilton, D. Reed and A. J. Welch, *J. Chem. Soc., Dalton Trans.*, 1990, 677.
36 R. N. Keller, H. D. Wycoff and L. E. Marchi, *Inorg. Synth.*, 1946, **2**, 1.
37 B. K. Teo and J. C. Calabrese, *Inorg. Chem.*, 1976, **15**, 2467.
38 *Crystallization of Nucleic Acids and Proteins*, eds. A. Ducruix and R. Giege, IRL Press, Oxford, 1992, p. 83.
39 D. J. Watkin, J. R. Carruthers and P. W. Betteridge, *CRYSTALS User Manual*, Chemical Crystallography Laboratory, University of Oxford, 1985.
40 S. R. Hall, F. H. Allen and I. D. Brown, *Acta Crystallogr., Sect. A*, 1991, **47**, 655.

41 G. M. Sheldrick, SHELXS 86, Program for the Solution of Crystal Structures, University of Göttingen, 1986.
42 J. R. Rollett, in *Crystallographic Computing*, ed. F. R. Ahmed, Munksgaard, Copenhagen, 1970, p. 171.
43 N. Walker and D. Stuart, *Acta Crystallogr., Sect. A.*, 1983, **39**, 158.

Received 27*th June* 1995; *Paper* 5/04139B